Improvement of Stability and Load Sharing in an Autonomous Microgrid Using Supplementary Droop Control Loop

Ritwik Majumder, *Student Member, IEEE*, Balarko Chaudhuri, *Member, IEEE*, Arindam Ghosh, *Fellow, IEEE*, Rajat Majumder, *Member, IEEE*, Gerard Ledwich, *Senior Member, IEEE* and Firuz Zare, *Senior Member, IEEE*

ABSTRACT: This paper investigates the problem of appropriate load sharing in an autonomous microgrid. High gain angle droop control ensures proper load sharing, especially under weak system conditions. However it has a negative impact on overall stability. Frequency domain modeling, eigenvalue analysis and time domain simulations are used to demonstrate this conflict. A supplementary loop is proposed around a conventional droop control of each DG converter to stabilize the system while using high angle droop gains. Control loops are based on local power measurement and modulation of the d-axis voltage reference of each converter. Coordinated design of supplementary control loops for each DG is formulated as a parameter optimization problem and solved using an evolutionary technique. The supplementary droop control loop is shown to stabilize the system for a range of operating conditions while ensuring satisfactory load sharing.

Index Terms: Autonomous Microgrid, Stability, Supplementary droop, Active and Reactive Power sharing.

I. INTRODUCTION

IN AN AUTONOMOUS microgrid, all the distributed generators (DGs) are responsible for maintaining the system voltage and frequency while sharing the active and reactive power. Load sharing without communication between converters is the most desirable option as the network can be complex and can span over a large geographic area. A common approach to achieve this is through the use of frequency droop characteristics so that the parallel converters can be controlled locally to deliver desired real and reactive power to the system. The real and reactive power sharing can be achieved by controlling two independent quantities – the frequency and the fundamental voltage magnitude [1, 2]. The impact of such load sharing on system stability has been explored in [3-6]. Transient stability of power system with the high penetration level of power electronics interfaced (converter connected) distributed generation is explored in [7]. The robust stability of a voltage and current control solution for a stand-alone DG unit is analyzed in [3] using structured singular values. This results in a discrete-time sliding mode current controller. In [5], the small-signal stability analysis of the combined droop and average power method for load sharing control of multiple distributed generation systems (DGs) in a stand-alone ac supply mode is discussed. The small-signal model is developed and its accuracy is verified from simulations of the original nonlinear model.

Modeling and analysis of autonomous operation of converter-based microgrid is presented in [6], in which the converters are controlled based on voltage and frequency droop. Each sub-module of the system is modeled in state-space form and all the modules are then combined together on a common reference frame. The model captures the detail of the control loops of the converter but not the switching action. Normal PI controllers are used for voltage and current control.

Droop control based on the angle of the output voltage, referred to as angle droop, is advantageous over the commonly used frequency droop. It is therefore adopted in this paper. Frequency regulation constraint limits the allowable range of frequency droop gain, which in turn, may lead to chattering during frequent load changes in a microgrid. Hence, for voltage source converter (VSC) based DGs, better load sharing can be done by drooping the converter output voltage angle instead of frequency. The application of angle controller in a converter interfaced DG is shown in [8]. This requires signals from global positioning system (GPS) for angle referencing, but no communication link between converters [9]. The initial angles are set based on the desired level of power sharing and the real power droop coefficients can be chosen depending on the maximum and minimum value of load demand and load sharing ratio. Moreover, the inclusion of linear quadratic regulator based state feedback controller makes reference following effective and shows a faster convergence compared to the frequency droop considered in [6].

It is shown that high values of angle droop gains are required to ensure proper load sharing, especially under weak system conditions. However, high droop gains have a negative impact on the overall stability of the system as illustrated through eigenvalue analysis and simulations. A supplementary control loop is proposed around the primary droop control loop to stabilize the system while ensuring proper load sharing. The control loops for each DG converter are based on local power measurement and modulation of the d-axis voltage reference.

The design of the supplementary controllers is formulated as a parameter optimization problem with constraints on the closed loop stability over a range of operating conditions. The structure of the controller is fixed *a priori* and the parameters are derived out of the optimum solution. Lack of reasonable initial guess prompted use of evolutionary technique for solving the optimization problem. The use of the proposed supplementary droop control loop stabilizes the system for a

Ritwik. Majumder, A. Ghosh, G. Ledwich and F. Zare are with the School of Engineering Systems, Queensland University of Technology, Brisbane, Australia,. B. Chaudhuri is with Department of Electrical and Electronic Engineering, Imperial College London, London, UK and Rajat. Majumder is with Power Technologies, ABB Corporate Research, Västerås, Sweden.

range of operating conditions while ensuring satisfactory load sharing.

The original contribution of this paper is in enabling the use of higher angle droop gains for improved load sharing. The negative impact on stability is addressed using the proposed supplementary control loop. Modeling, eigenvalue analysis, control design through parameter optimization and time domain simulations are used to illustrate the claims. The proposed control is aimed for a microgrid with only converter interfaced DG and in presence of inertial DGs, where the rate of power output is determined by machine inertia, the control law has to be modified.

II. Converter Structure and Control

The important variables that are used in the remainder of the paper are listed below.

v_{cf}	converter output voltage
i_2	converter output current
i_{cf}	converter filter capacitor current
K_1, K_2, K_3	state feedback gains
v_t	network voltage
δ	converter output voltage angle
P, Q	converter real and reactive power output
ω_C	low pass filter cut off frequency
m, n	droop controller gains

Also note that uppercase letters indicate rms values, while the lowercase letters indicate instantaneous values.

All the DGs are assumed to be an ideal dc voltage source supplying a voltage of V_{dc} to the VSC. The structure of the VSC is shown in Fig. 1. The VSC contains three H-bridges that are supplied from the common dc bus. The outputs of the H-bridges are connected to three single-phase transformers that are connected in wye for required isolation and voltage boosting [10]. The resistance R_T represents the switching and transformer losses, while the inductance L_T represents the leakage reactance of the transformers. The filter capacitor C_f is connected to the output of the transformers to bypass switching harmonics, while L_f represents the output inductance of the DG source.

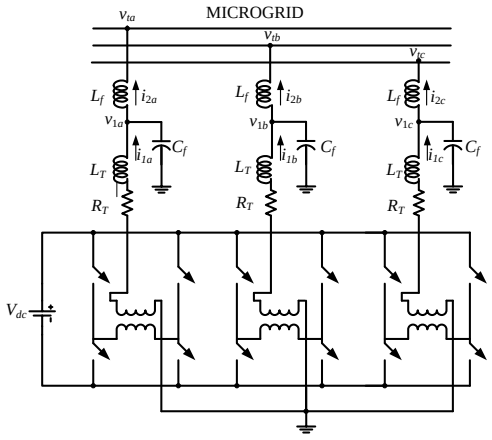


Fig. 1. Converter structure.

The equivalent circuit of one phase of the converter is shown in Fig. 2. In this, $u \cdot V_{dc}$ represents the converter output voltage, where u is the switching function and is given by $u = \pm 1$. The main aim of the converter control is to generate u. From the circuit of Fig. 2, the following state vector is chosen

$$x^T = \begin{bmatrix} i_2 & i_{cf} & v_{cf} \end{bmatrix} \tag{1}$$

where converter output voltage is the same as the voltage across the filter capacitor v_{cf}. Then the state space description of the system can be given as

$$\dot{x} = Ax + Bu \tag{2}$$

The discrete-time equivalent of (2) is

$$x(k+1) = Fx(k) + Gu(k) \tag{3}$$

The control law is then given by

$$u_c(k) = -K\left[x(k) - x_{ref}(k)\right] \tag{4}$$

$$\begin{aligned} &\text{If } u_c(k) > h \text{ then } u = +1 \\ &\text{elseif } u_c(k) < -h \text{ then } u = -1 \end{aligned} \tag{5}$$

where h is a small number, K is a gain matrix and x_{ref} is the reference vector. The gain matrix, in this paper, is obtained through linear quadratic regulator (LQR) design. The above control action results in perfect tracking when the error is within limit [11]. For the model derivation of the next section, the switching action is neglected.

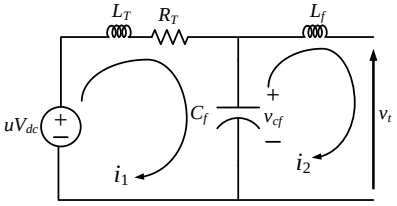


Fig. 2. Single-phase equivalent circuit of VSC.

III. Droop Control, DG Reference Generation and Power Sharing

The same control strategy, as discussed in this section, is applied to all the DGs. It is assumed the total power demand in the microgrid can be supplied by the DGs and no load shedding is required. The output voltages of the converters are controlled to share this load proportional to the rating of the DGs. As an output inductance is connected to each of the VSCs, the real and reactive power injection from the DG source to the microgrid can be controlled by changing voltage magnitude and its angle [1-4]. Fig. 3 shows the power flow from a DG to the microgrid where the rms values of the voltages and current are shown and the output impedance is denoted by jX_f. It is to be noted that real and reactive power (P and Q) shown in this figure are average values.

A. Droop Control

The instantaneous real and reactive powers, denoted by p and q respectively, from the DG to the microgrid can be calculated as

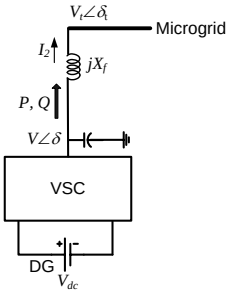


Fig. 3. Microgrid-DG connection,

$$P = \frac{V \times V_t \sin(\delta - \delta_t)}{X_f}$$
$$Q = \frac{V^2 - V \times V_t \cos(\delta - \delta_t)}{X_f} \quad (6)$$

These instantaneous powers are passed through low pass filters to obtain the average real and reactive power P and Q. It is to be note that the VSC does not have any direct control over $V_t\angle\delta_t$. Hence from (6), it is clear that if the angle difference $(\delta - \delta_t)$ is small, the real power can be controlled by controlling δ, while the reactive power can be controlled by controlling V. Thus the power requirement can be distributed among the DGs, similar to conventional droop by dropping the voltage magnitude and angle as

$$\delta = \delta_{rated} - m \times (P - P_{rated})$$
$$V = V_{rated} - n \times (Q - Q_{rated}) \quad (7)$$

where V_{rated} and δ_{rated} are the rated voltage magnitude and angle respectively of the DG, when it is supplying the load to its rated power levels of P_{rated} and Q_{rated}. The coefficients m and n respectively indicate the voltage angle drop vis-à-vis the real power output and the magnitude drop vis-à-vis the reactive power output. These values are chosen to meet the voltage regulation requirement in the microgrid. The coefficient values for different DGs are chosen such that they share the load in proportion to their rating. Let us assume that there are a total number of Z DGs in the system and their droop coefficients are denoted by $m_1, \ldots, m_Z$ and $n_1, \ldots, n_Z$. Then the power sharing between the DGs can be given as

$$m_1 \times P_{1rated} = \cdots = m_Z \times P_{Drated}$$
$$n_1 \times Q_{1rated} = \cdots = n_Z \times Q_{Drated} \quad (8)$$

B. DG Reference Generation

It is evident from (4) that the reference for all the elements of the states, given in (1), is required for state feedback. Since V and δ are obtained from the droop equation (7), the reference for the capacitor voltage and current are given by

$$v_{cfref} = V \cos(\omega t + \delta) \quad (9)$$
$$i_{cfref} = V\omega C_f \sin(\omega t + \delta) \quad (10)$$

The reference for the current i_2 can be calculated as

$$i_{2ref} = \frac{v_{cf} - v_t}{jX_f} \quad (11)$$

The above equation will need a phase shifter for the calculation of the instantaneous current reference. This may not be desirable. Hence the measured values of the average real and reactive power output of the VSC can be used to find the magnitude and phase angle of the reference rms current. From Fig. 3, it can be seen that

$$\left|I_{2ref}\right| = \frac{\sqrt{P^2 + Q^2}}{V_{cf}} \text{ and } \angle I_{2ref} = \delta - \tan^{-1}(Q/P)$$

Hence the current reference can be given as

$$i_{2ref} = \left|I_{2ref}\right| \cos(\omega t + \angle I_{2ref}) \quad (12)$$

It is to be noted that all the converters are operated in a fixed frequency of 50 Hz and the angles are controlled with reference to a common 50 Hz reference.

C. Power Sharing with Angle Droop

To show the power sharing with angle droop, two DGs and a load are considered as shown in Fig. 4.

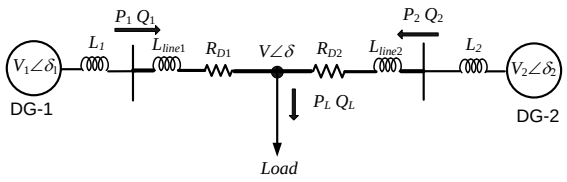


Fig. 4. Power Sharing with Angle Droop.

The voltages and the power flow are indicated in the figure. Applying DC load flow with all the necessary assumptions we get,

$$\delta_1 - \delta = (\lambda_1 + \lambda_{L1})P_1$$
$$\delta_2 - \delta = (\lambda_2 + \lambda_{L2})P_2 \quad (13)$$

where $\lambda_1 = \omega L_1/(V_1V)$, $\lambda_{L1} = \omega L_{Line1}/(V_1V)$, $\lambda_2 = \omega L_2/(V_2V)$ and $\lambda_{L2} = \omega L_{Line2}/(V_2V)$.

The angle droop equation of the DGs are given by

$$\delta_1 = \delta_{1rated} - m_1 \times (P_{1rated} - P_1)$$
$$\delta_2 = \delta_{2rated} - m_2 \times (P_{2rated} - P_2) \quad (14)$$

The offset in the angle droop are taken such that when DG output power is zero, the DG source angle is zero. For that, the rated droop angles are taken as $\delta_{1rated} = m_1P_{1rated}$ and $\delta_{2rated} = m_2P_{2rated}$. Then from (14), we get

$$\delta_1 - \delta_2 = m_1P_1 - m_2P_2 \quad (15)$$

Similarly from (13), we get

$$\delta_1 - \delta_2 = (\lambda_1 + \lambda_{L1})P_1 - (\lambda_2 + \lambda_{L2})P_2 \quad (16)$$

Assuming the system to be lossless, we can find from Fig. 4 that $P_2 = P_L - P_1$ and substituting this (15) and (16) we get,

$$(\lambda_1 + \lambda_{L1})P_1 - (\lambda_2 + \lambda_{L2})(P_L - P_1) = m_1P_1 - m_2(P_L - P_1)$$
$$\Rightarrow P_1 = \frac{\lambda_2 + \lambda_{L2} + m_2}{\lambda_2 + \lambda_{L2} + m_2 + \lambda_1 + \lambda_{L1} + m_1} \quad (17)$$

Similarly P_2 can be calculated as

$$P_2 = \frac{\lambda_1 + \lambda_{L1} + m_1}{\lambda_2 + \lambda_{L2} + m_2 + \lambda_1 + \lambda_{L1} + m_1} \tag{18}$$

From (17) and (18), the ratio of the output power is calculated as,

$$\frac{P_1}{P_2} = \frac{\lambda_2 + \lambda_{L2} + m_2}{\lambda_1 + \lambda_{L1} + m_1} \tag{19}$$

It is to be noted that the values of λ_1 and λ_2 are small compared to the value of m_1 and m_2. The value of the feedback gain (m_1=1x10-6) should be compared with the $\lambda_1 = \omega L_1/(V_1 V)$ and $\lambda_L = \omega L_{Line1}/(V_1 V)$. For an 11 KV system, the calculated value of λ_1 for DG-1 is 0.19 x10-6, while λ_{L1} is 0.039 x10-6 and both are smaller than m_1. However, the output inductances are also chosen as inversely proportional to the power rating of the DGs. Thus the error in proportional power sharing is due to line inductances (as per 19) and it is very small. Moreover the microgrid line is considered to be mainly resistive with low line inductance and the DG output inductance is much larger, and hence we can write

$$m_1 >> \lambda_1 >> \lambda_{L1} \text{ and } m_2 >> \lambda_2 >> \lambda_{L2}$$

Therefore from (18) it is evident that the droop coefficients play the dominant role in the power sharing. As the droop coefficients are taken as inversely proportional to the DG rating, from (18) we can write

$$\frac{P_1}{P_2} \approx \frac{m_2}{m_1} = \frac{P_{1rated}}{P_{2rated}} \tag{20}$$

The error is further reduced by taking the output inductance (L_1, L_2) of the DGs inversely proportional to power rating of the DGs. If the microgrid line is inductive in nature, and of high value, then the network knowledge is needed to minimize the error by choosing the DG output inductance such that

$$\frac{\lambda_1 + \lambda_{line1}}{\lambda_2 + \lambda_{line2}} = \frac{P_{2rated}}{P_{1rated}}$$

The system shown in Fig. 4 is a very simple example to show the power sharing. In a real system with number of DGs and loads in different location line impedance will have an impact on the load sharing. But for a microgrid within a small geographical area, the line inductance will never be very high. Moreover a high droop coefficient will always play a dominant role and will enable desired sharing with a very small deviation. A comparison of angle droop with traditional frequency is given in Appendix B.

It is to be noted that if the GPS signal is lost for one of the generator for several seconds, then the local clock can be sufficient for satisfactory operation. This is possible since a local clock can provide a reasonable representation of GPS time tag for tens of seconds but eventually the operating point shift in response to load change will cause degradation in power sharing. If this loss of signal continues then this unit can not participate in system wide load sharing and must revert to local load support or tripped. If there is sufficient concern about system wide loss of GPS reference signal, then a radio reference signal could be used.

IV. State Space Model of Autonomous Microgrid

The stability of a microgrid with high droop gains needs to be studied through the analysis of state-space models, and so suitable models of converters are needed to complement the well-established models of rotating machines. As machine models include features such as automatic voltage regulators and wash-out functions, the converter model should also include the internal control loops [12]. In an autonomous microgrid that contains converter based DGs only, the fast switching action can influence the network dynamics [6]. Hence the network is modeled by differential equation rather than algebraic equations for stability investigation. So far we have presented the single-phase control of the converter. However, for the analysis of the total microgrid system, a common reference frame is chosen and the system voltages and currents are converted in a DQ reference frame.

Fig. 5 shows the block diagram of the complete microgrid system containing Z DGs. It is assumed that the model of each of the DGs is the same. This includes the VSC with its state feedback controller, droop controller and the interface block that connects the converter to the network. The system equations are nonlinear and thus they are linearized to perform eigenvalue analysis. The linear quantities are denoted by the prefix Δ. The measured real and reactive power output (ΔP, ΔQ) of converter is fed to the droop controller, while voltage reference (Δv_{cfref}, $\Delta \delta_{ref}$), set by droop controller, is fed back to the converter. The DGs are connected to the network through the interface block which converts the input/output signal from DG reference frame to the common reference frame and vice versa. Each DG block has current output to the network, which is converter output current (Δi_{2D}, Δi_{2Q}) and network voltage as input (Δv_{tD}, Δv_{tQ}). Similarly, the input to the load model is the network voltage at the connected nodes (Δv_{tD}, Δv_{tQ}) and its output is the load current (Δi_{LoadDQ}). The state space equations of the DG-VSC, load and network are derived separately in a modular fashion. These are then combined together depending on the network structure to get the overall microgrid system model.

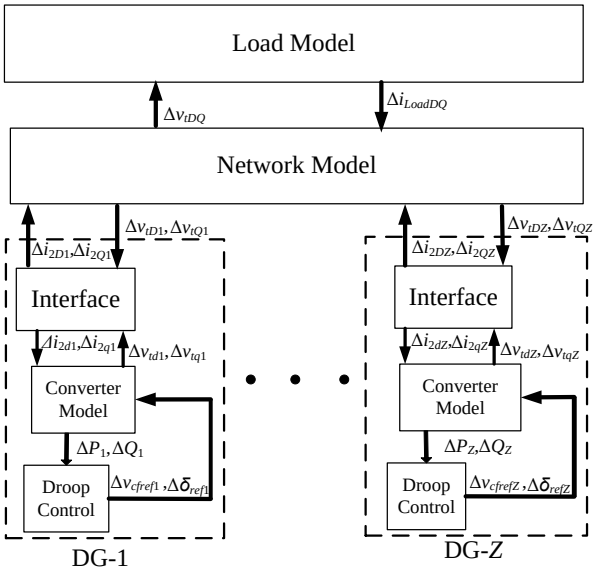


Fig. 5. Interconnection diagram of the complete microgrid system.

A. Converter Model

From equivalent circuit shown in Fig. 2, the following equations are obtained for each of the phases of the three-phase system

$$\frac{di_1}{dt} = -\frac{R_T}{L_T} i_1 + \frac{\left(-v_{cf} + u.V_{dc}\right)}{L_T} \tag{21}$$

$$\frac{dv_{cf}}{dt} = \frac{\left(i_1 - i_2\right)}{C_f} \tag{22}$$

$$v_{cf} - v_t = L_f \frac{di_2}{dt} \tag{23}$$

Equations (21-23) are translated into a *d-q* reference frame of converter output voltages, rotating at system frequency ω,

Defining a state vector as

$$x_i = [i_{1d} \quad i_{1q} \quad i_{2d} \quad i_{2q} \quad v_{cfd} \quad v_{cfq}]^T$$

the state equation in the *d-q* frame is given by

$$\dot{x}_i = A_i x_i + B_1 u_{cdq} + B_2 v_{tdq} \tag{24}$$

It is assumed here that the tracking is perfect and hence, in the limit, u can be represented by u_c. From (4), u_{cdq} can be expressed as

$$\begin{aligned} u_{dq} &= -k_1\left(i_{2dq} - i_{2refdq}\right) - k_2\left(i_{1dq} - i_{2dq} - i_{cfrefdq}\right) \\ &\quad - k_3\left(v_{cfdq} - v_{cfrefdq}\right) \\ &= -k_2 i_{1dq} + \left(k_2 - k_1\right) i_{2dq} - k_3 v_{cfdq} + k_1 i_{2refdq} \\ &\quad + k_2 i_{cfrefdq} + k_3 v_{cfrefdq} \end{aligned} \tag{25}$$

The above equation can be written in matrix form as

$$\begin{bmatrix} u_d \\ u_q \end{bmatrix} = G_i x_i + H_i y_{refdq} \tag{26}$$

where,

$$y_{refdq} = [i_{2refd} \quad i_{2refq} \quad i_{cfrefd} \quad i_{cfrefq} \quad v_{cfrefd} \quad v_{cfrefq}]^T$$

Substituting (26) into (24) we get

$$\dot{x}_i = \left(A_i + B_1 G_1\right) x_i + B_1 H_i y_{refdq} + B_2 v_{tdq} \tag{27}$$

Since V_{dc} is assumed to be constant, the linearization of (27) will not alter B_1. This linearization results in

$$\Delta\dot{x}_i = A_{CONV}\, \Delta x_i + B_{CONV}\, \Delta y_{refdq} + B_2 \Delta v_{tdq} \tag{28}$$

where , $A_{CONV} = A_i + B_1 G_i$ and $B_{CONV} = B_i H_i$.

The current reference can be expressed in terms of the voltage reference as

$$\begin{bmatrix} \Delta i_{cfrefd} \\ \Delta i_{cfrefq} \end{bmatrix} = \begin{bmatrix} 0 & -\omega C_f \\ \omega C_f & 0 \end{bmatrix} \begin{bmatrix} \Delta v_{cfrefd} \\ \Delta v_{cfrefq} \end{bmatrix} \tag{29}$$

$$\begin{bmatrix} \Delta i_{2refd} \\ \Delta i_{2refq} \end{bmatrix} = \begin{bmatrix} 0 & \frac{1}{\omega L_f} \\ -\frac{1}{\omega L_f} & 0 \end{bmatrix} \begin{bmatrix} \Delta v_{cfrefd} \\ \Delta v_{cfrefq} \end{bmatrix} + \begin{bmatrix} 0 & \frac{1}{\omega L_f} \\ -\frac{1}{\omega L_f} & 0 \end{bmatrix} \begin{bmatrix} \Delta v_{td} \\ \Delta v_{tq} \end{bmatrix} \tag{30}$$

Combining (29) and (30), the reference vector is given as

$$y_{refdq} = M_1 \Delta v_{cfrefdq} + M_2 \Delta v_{tdq} \tag{31}$$

Combing (28) and (31) we get the converter model as

$$\Delta\dot{x}_i = A_{CONV}\, \Delta x_i + B_T \Delta v_{cfrefdq} + B_{BUS} \Delta v_{tdq} \tag{32}$$

where $B_T = B_{CONV} M_1$ and $B_{BUS} = B_{CONV}\,(M_2 + B_2)$.

B. Droop Controller

The droop controller sets the references for converter output voltage magnitude and its angle. The output voltage of the converter is equal to voltage across the capacitor C_f. The measured instantaneous real and reactive power are passed through two lowpass filters to obtain the average values of P and Q respectively. These can be expressed as

$$\begin{aligned} P &= \frac{\omega_C}{s + \omega_C}\, p = \frac{\omega_C}{s + \omega_C}\left(v_{cfd} i_{2d} + v_{cfq} i_{2q}\right) \\ Q &= \frac{\omega_C}{s + \omega_C}\, q = \frac{\omega_C}{s + \omega_C}\left(v_{cfd} i_{2q} - v_{cfq} i_{2d}\right) \end{aligned} \tag{33}$$

where ω_c is cut-off frequency of the filter. Linearizing equation (33) we get,

$$\begin{bmatrix} \Delta\dot{P} \\ \Delta\dot{Q} \end{bmatrix} = \begin{bmatrix} -\omega_C & 0 \\ 0 & -\omega_C \end{bmatrix} \begin{bmatrix} \Delta P \\ \Delta Q \end{bmatrix} + B_P \begin{bmatrix} \Delta v_{cfdq} \\ \Delta i_{2dq} \end{bmatrix} \tag{34}$$

Let us now define the three-phase reference filter capacitor voltages as

$$\begin{aligned} v_a &= V_{cfref} \cos(\omega t), \quad v_b = V_{cfref} \cos(\omega t - \frac{2\pi}{3}) \\ v_c &= V_{cfref} \cos(\omega t + \frac{2\pi}{3}) \end{aligned} \tag{35}$$

From the above equation we get

$$v_{cfrefd} = V_{cfref} \quad \text{and} \quad v_{cfrefq} = 0 \tag{36}$$

It can be seen from Fig. 3 that v_{cf} is the converter output voltage. Hence from (7) and (36), we can write the voltage droop equation as

$$v_{cfrefd} = V_{cfref} = V_{rated} - n\left(Q - Q_{rated}\right) \tag{37}$$

Linearizing and combining (7) and (37) them we get the droop controller model as

$$\begin{bmatrix} \Delta\delta_{ref} \\ \Delta v_{cfrefd} \\ \Delta v_{cfrefq} \end{bmatrix} = \begin{bmatrix} 0 & -m & 0 \\ 0 & 0 & -n \\ 0 & 0 & 0 \end{bmatrix} \begin{bmatrix} \Delta\delta \\ \Delta P \\ \Delta Q \end{bmatrix} \tag{38}$$

C. Combined Converter-Droop Control Model

Let us now substitute $\Delta V_{cfrefdq}$ from (38) in the converter model of (32). This gives

$$\Delta \dot{x}_i = A_{CONV}\,\Delta x_i + B_G \begin{bmatrix} \Delta P \\ \Delta Q \end{bmatrix} + B_{BUS}\,\Delta v_{tdq} \tag{39}$$

Combining the converter and droop controller state vectors together an extended state vector is formed as

$$x_{CONV} = \begin{bmatrix} P & Q & i_{1d} & i_{1q} & i_{2d} & i_{2q} & v_{cfd} & v_{cfq} \end{bmatrix}^T$$

The combined state equation is then written as

$$\Delta \dot{x}_{CONV} = A_c \Delta x_{CONV} + B_c \Delta v_{tdq} \tag{40}$$

D. Transformation to Common Reference Frame

Since all the converters are modeled individually with their own *d-q* axis reference, they need to be transformed into common reference *D-Q* frame. The small signal output current of the converter in *D-Q* frame is

$$\Delta i_{2DQ} = T_S\,\Delta i_{2dq} + T_C\,\Delta\delta \tag{41}$$

Similarly the input to the converter from the network, the network voltage can be expressed in as,

$$\Delta V_{tdq} = T_S^{-1}\Delta v_{tDQ} + T_V^{-1}\Delta\delta \tag{42}$$

Substituting equation (42) in (40) we get

$$\Delta \dot{x}_{CONV} = A_c \Delta x_{CONV} + B_L \Delta v_{tDQ} + B_{P1}\Delta\delta \tag{43}$$

where $B_L = B_C\,T_S^{-1}$ and $B_{P1} = B_C\,T_V^{-1}$

It is to be noted that $\Delta\delta$ in equation (43) can be expressed as the droop controller output equation in terms of ΔP. It is assumed that the change in angle in the converters is instantaneous such that the converter produces the demanded angle (δ_{ref}). The state equation (43) can be written as

$$\Delta \dot{x}_{CONV} = A_L \Delta x_{CONV} + B_L \Delta v_{tDQ} \tag{44}$$

where $A_L = A_c - m\begin{bmatrix} B_{P1} & O_{8\times 7} \end{bmatrix}$. Similarly (41) is expressed as

$$\Delta i_{2DQ} = C_P\,\Delta X_{CONV} \tag{45}$$

Let us assume that the microgrid has *Z* number of DGs with their state space and output equations being given by (44-45) as

$$\left.\begin{aligned} \Delta \dot{x}_{CONVi} &= A_{Li}\Delta x_{CONVi} + B_{Li}\Delta v_{tDQi} \\ \Delta i_{2DQi} &= C_{Pi}\Delta X_{CONVi} \end{aligned}\right\}, i = 1,\ldots,Z \tag{46}$$

Then the combined state space equation including all the converters in the system is written as

$$\begin{aligned} \Delta \dot{x}_Z &= A_Z \Delta x_Z + B_Z \Delta v_{tZ} \\ \Delta i_{2Z} &= C_Z \Delta x_Z \end{aligned} \tag{47}$$

The network and loads are then modeled and combined with (47) to get a homogenous state equation of the form

$$\Delta \dot{x}_T = A_T \Delta x_T \tag{48}$$

where x_T is the total state vector of the microgrid system. The derivation of (48) is not shown here. The eigenvalues of the matrix A_T describes the closed-loop stability of the system.

V. System Structure and Eigenvalue Analysis of Microgrid

The structure of the study system is shown in Fig. 6. The real and reactive powers supplied by the DGs are denoted by P_i, Q_i, i = 1, …, 4. The real and reactive power demand from the loads are denoted by P_{Li}, Q_{Li}, i = 1, …, 5. The line impedances are denoted by Z_{12}-Z_{89} in the figure. The system matrix A_T is derived with all the parameter shown in Table-I for eigenvalue analysis.

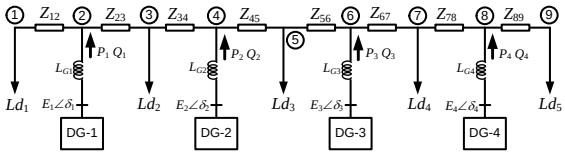


Fig. 6. Microgrid system under consideration.

We shall term the system to be operating under nominal condition when the system operates with the parameters given in Table-I. The droop gains for the nominal condition are smaller. The eigenvalues of the system for this nominal operating condition are shown in Fig. 7. It can be seen that the eigenvalues, based on their damping (real component), are placed on four different clusters. It will be shown that the dominant eigenvalues of cluster 1 are sensitive to the changes in the droop controller parameters. The eigenvalues of clusters 2, 3 and 4 are sensitive to the other parameters, like filter, state feedback controller, load etc., and their effects are not investigated here.

Fig. 8 shows the locus of the eigenvalues of cluster 1 as the droop controller real power coefficient *m* changes. Note that both the complex conjugate pairs are not shown here. It can be seen that for a very high value of *m* (0.11×10^{-5}), a complex conjugate pair of eigenvalues almost reaches the imaginary axis indicating a low system stability. For $m = 0.15\times10^{-5}$, the above pair crosses the imaginary axis and one more eigenvalues pair crosses imaginary axis, indicating an unstable operation.

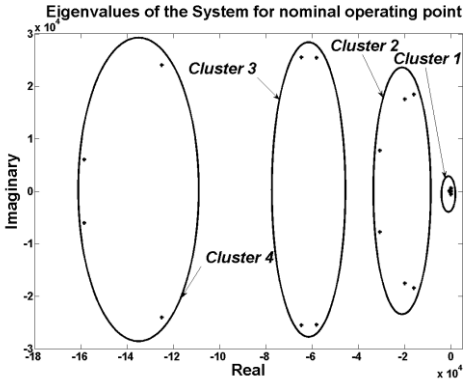


Fig. 7. Eigenvalues for nominal operating condition.

TABLE-I: NOMINAL SYSTEM PARAMETERS

System Quantities	Values
Systems frequency	50 Hz
Feeder impedance $Z_{12} = Z_{23} = Z_{34} = Z_{45} = Z_{45} = Z_{56} = Z_{67} = Z_{78} = Z_{89}$	1.03 + *j* 4.71 Ω
Load ratings	
Ld_1	100 kW and 90 kVAr
Ld_2	120 kW and 110 kVAr
Ld_3	80 kW and 68 kVAr
Ld_4	80 kW and 68 kVAr
Ld_5	90 kW and 70 kVAr
DG ratings (nominal)	
DG-1	100 kW
DG-2	200 kW
DG-3	150 kW
DG-4	150 kW
Output inductances	
L_1	75 mH
L_2	37.5mH
L_3	56.4 mH
L_4	56.4mH

System Quantities	Values
DGs and VSCs	
DC voltages (V_{dc1} to V_{dc4})	3.5 kV
Transformer rating	3 kV/11 kV, 0.5 MVA, 2.5%
VSC losses (R_f)	L_f
Filter capacitance (C_f)	1.5 Ω
Hysteresis constant (h)	50 μF
	10^{-5}
Droop Coefficients	
Power–angle	
(Lower Droop Gains)	
m_1	0.1 rad/MW
m_2	0.05 rad/MW
m_3	0.075 rad/MW
m_4	0.075 rad/MW
Power–angle	
(Higher Droop Gains)	
m_1	1.0 rad/MW
m_2	0.5 rad/MW
m_3	0.75 rad/MW
m_4	0.75 rad/MW
Voltage–Q	
n_1	0.04 kV/MVAr
n_2	0.02 Kv/MVAr
n_3	0.03 Kv/MVAr
n_4	0.03 Kv/MVAr

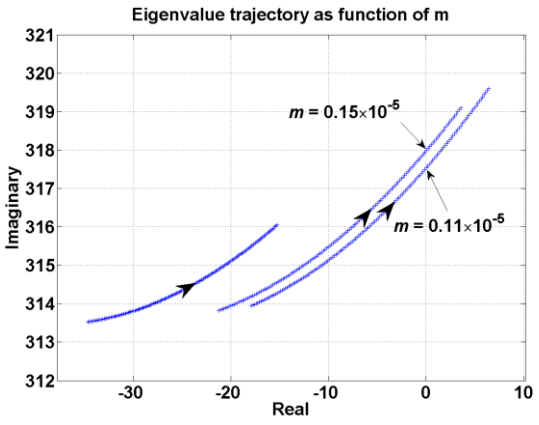


Fig. 8. Eigenvalue locus with real power droop gain change.

It is to be mentioned here that the gains of the state feedback controllers have no adverse effects on the system stability. The controllers are designed using LQR, which is very robust. This has been observed by changing the cost function in the LQR design and the results are not shown here.

VI. Suppelementary Droop Control Loop

The schematic layout of the supplementary loop around the conventional droop control is shown in Fig. 9. The real power output P_i, of the i^{th} converter is fed through a high pass washout circuit (with 0.05 s time constant) to capture the oscillatory behavior, eliminating the dc component, ΔP_i about the steady-state value P_i. The supplementary control signal, Δv_{drefi}, modulates the output of the droop controller to generate a modified d-axis voltage reference, v_{drefi}' for each converter. Equation (7) is then modified for the i^{th} converter as

$$\begin{aligned} \delta_i^* &= \delta_i + \Delta\delta_i = \delta_{irated} - m \times (P_i - P_{irated}) + \Delta\delta_i \\ V_i^* &= V_i + \Delta V_i = V_{irated} - n \times (Q_i - Q_{irated}) + \Delta V_i \end{aligned} \quad (49)$$

where ΔV_i and $\Delta\delta_i$ are the voltage magnitude and voltage angle correction by the supplementary controller signal $\Delta V_{drefi.}$ The resultant voltage reference for the converter is

$$V_i^* \angle \delta_i^* = V_{drefi}' + j * V_{qrefi} \quad (50)$$

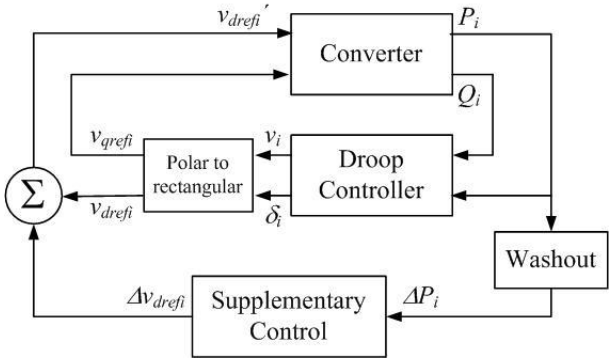


Fig. 9. Supplementary Droop Controller Configuration

When the DGs are supplying rated power, the angle of the converter output voltage is $\delta_{rated.}$ As the $\delta_{irated} = m_i P_{irated}$, the rated angles for all the DGs are 0.1 rad,. It is to be noted that the rated angles are chosen so that when the output power of the DGs are zero, the reference output voltage angle is zero.

The test system considered for this study has three critical oscillatory modes with frequencies in the vicinity of 50 Hz which require stability enhancement. To ensure adequate controllability and observability of these modes, each of the four converters were equipped with a separate supplementary control loop. The structure of each controller was fixed a priori and is comprised of three lead-lag blocks and a gain as shown in Fig. 10 for the i^{th} converter. The calculation of these unknown gains, K_i, i=1,2,3,4, and the time constants T_{ij}, i =1,2,3,4; j = 1,2,..,6, are formulated as a parameter optimization problem with the constraint on stability of the closed-loop over a range of operating conditions. A lower limit of 0.01 and an upper limit of 100 were imposed on the search space of the denominator time constants to ensure stable poles and fast enough controller response. Simultaneous design of the four

decentralized controllers eliminates possible interactions and ensures overall stability due to their combined action.

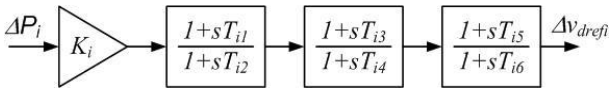


Fig. 10. Supplementary controller structure

It is not straight forward to solve the above parameter optimization problems using analytical techniques [13, 14], one of the reasons being lack of proper choice of initial guess. Hence, swarm optimization [15] – one of the standard evolutionary techniques – was employed here. The optimum gains and time constants obtained are shown in Table II. Parameters of the supplementary controllers are tuned simultaneously to eliminate possible interactions. No constraint on gain of the controller and lead time constant of each lead-lag compensator block have been imposed during the optimization stage to allow more search space. This has resulted in one negative gain and a few right half plane zeros in the compensator. If the phase compensation required is less than zero, it is more effective (in terms of the number of lead-lag blocks required) to use a negative feedback (180 degrees) and to compensate for only the difference between 180 degrees and original phase compensation. For the first channel with negative gain (K_1) this turned out to be the case. Also a non minimum phase feedback controller does not imply a non minimum phase closed loop system. The step responses did not show any evidence of non minimum phase behavior. Constraining feedback to be minimum phase for this problem with a wide range of droop gains resulted in no feasible solution. Permitting non minimum phase feedback enabled a feasible solution to be found. If there were less onerous requirement on the range of gain then a feasible solution become possible with a minimum phase constraint. However we placed the major emphasis in accurate sharing and the optimization process results in right half plane zeros as mentioned above.

A standard lead lag compensation structure, which is most widely adopted and easily implementable structure of different kind of supplementary controllers in power system application such as PSS (Power System Stabilizer), is adopted during control design.

Table-II: Parameters of the supplementary droop control loop

Parameters	Conv 1	Conv 2	Conv 3	Conv 4
K_i	-13.8409	4.8089	12.3064	12.4806
T_{i1}	13.1384	-12.805	14.6033	14.8943
T_{i2}	8.6429	12.4003	13.9471	1.0895
T_{i3}	15.6881	16.1046	-1.1439	-14.482
T_{i4}	0.3669	0.01	6.1067	0.01
T_{i5}	3.8954	5.2054	0.01	0.4818
T_{i6}	0.2475	0.4223	0.01	5.9059

As high droop gains are needed for proper load sharing, the proposed supplementary controller is aimed to guarantee the system stability even with high droop gains. Fig. 11 shows the close loop eigenvalue trajectory as function of *m* for the similar variation as in Fig. 8. It can be seen that with the proposed controller, the eigenvalues stays in the left side of the S plane indicating stable operation of the system. Note that the controller gains were optimized to obtain a good performance over a range of operating conditions despite the requirement of stabilizing a family of a number of unstable plants with a fixed structure low order compensator. This has resulted in the change of frequencies of the dominant eigenvalues. However, as the frequencies did not migrate either up to the switching range or down to the low oscillatory frequency range, it was not necessary to modify the performance index to avoid the frequency shift.

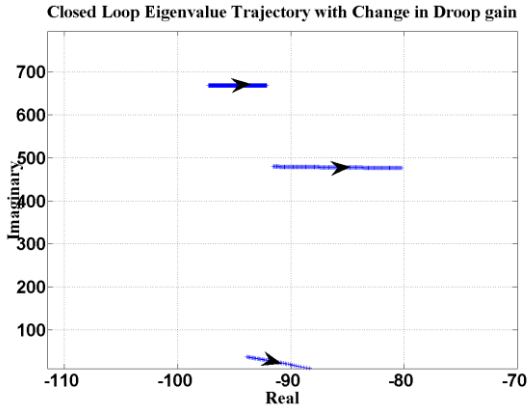


Fig. 11. Eigenvalue locus with the change in real droop gain

VII. Simulation Studies

Simulation studies are carried out in PSCAD/EMTDC (version 4.2). Different configurations of load and power sharing of the DGs are considered. The DGs are considered as inertia less dc source supplied through a VSC. The system data used for eigenvalue analysis (Table-I) are also used here. The lower and higher values of the droop controller parameter are shown in Table-I. The numerical values of simulation results are shown in Appendix-A, Table-III. The power sharing ratios, along with the desired ratios (indicated within parentheses) and the mean error in power sharing with and without supplementary controllers are shown in the table.

A. Case 1: Full System of Fig. 6 with Lower Droop Gains

In this case, it is assumed that all the DGs and loads are connected to the microgrid as shown in Fig. 6. The lower droop gains values of controller parameters, given in Table-1, are considered here. With the system operating in the steady state, Ld_1 changed to 155 kW from 100 kW at 0.25 s. Fig. 12 (a) shows the real power sharing while Fig. 12 (b) shows the three phase terminal voltages of DG-1. It can be seen that the controller provides proper load sharing with stable system operation.

B. Case 2: Reduced System with Lower Droop Gains

To investigate the load sharing with reduced system, DG-2 and DG-3 are disconnected at 0.25 s and the total power is shared by DG-1 and DG-4 as shown in Fig. 13. At 1.3 s, Ld_2 Ld_3, Ld_4 and Ld_5 are also disconnected. The two DGs connected to the microgrid supply the 100 kW load, Ld_1. It can be seen that system operation is stable. However due to weak system condition, as the DGs are located geographically far

from each other, they can not share load in the desired ratio of 1:1.33 (see Table-III, Appendix A).

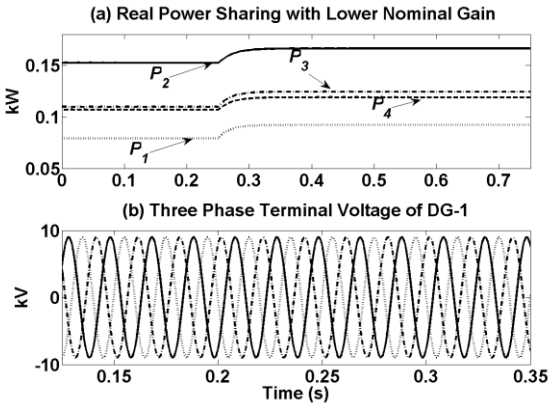


Fig. 12. Real and reactive power during a change in load 1.

C. Case 3: System Stability with High Droop Gain

As discussed before in Section III.C, the power sharing can be made independent of the system condition and the converter output reactance by choosing high droop controller gains. The eigenvalue analysis, on the other hand, predicted system instability for such gains. To investigated the system stability with high droop gain, the full system (Case-1) is operated first with lower value of droop gain and at 0.2 s, the droop gains are changed to higher values as mentioned in Table-I. Fig. 14 (a) shows the system response with only droop controller while Fig. 14 (b) shows system response with proposed supplementary droop controller. The response validate the eigenvalue analysis of Figs. 8 and 11, where it is predicted that stable operation with high droop gains are possible with the proposed supplementary controller.

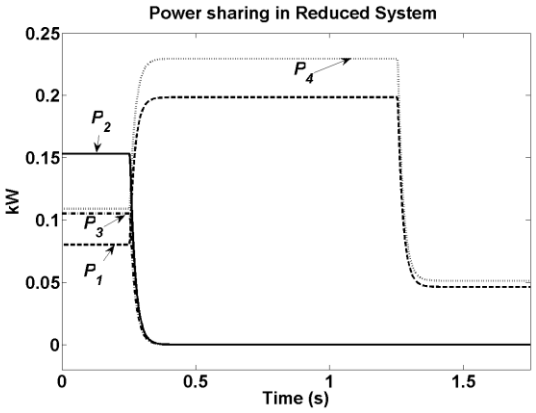


Fig. 13.Power sharing with reduced system

D. Case 4: Power Sharing with the Proposed Supplementary Controller

In this section, we shall investigate the load sharing capability with proposed supplementary controller and the system stability. All the simulations are done with high droop controller gain as mentioned in Table-I. With the system running in steady state and supplying power to all the loads, Ld_5 is disconnected from the microgrid at 0.25 s. Fig. 15 shows the system response. The power output of all the converters reduces proportionally and system attains steady state within 8-10 cycles. The droop controller converter output voltage reference angle and supplementary controller d-axis voltage modulation is shown in Fig. 16, which clearly shows a damping type controller with 90° phase shift during transients.

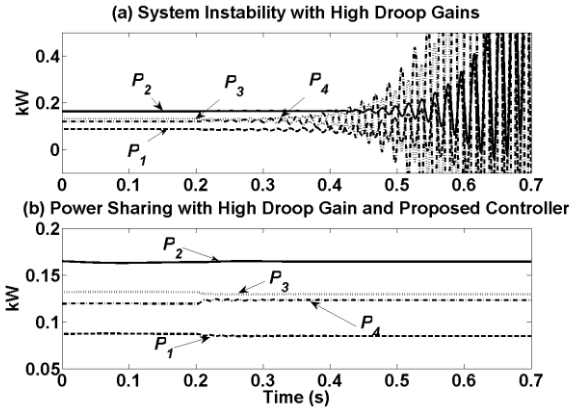


Fig. 14. System stability with high droop gain.

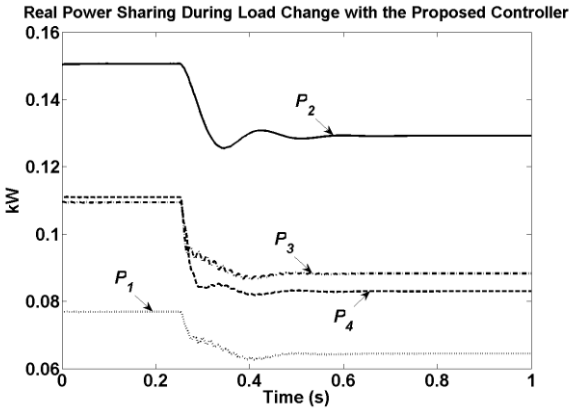


Fig. 15. Power sharing with proposed controller.

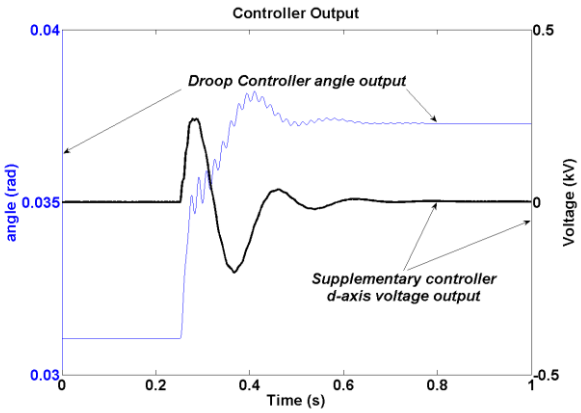


Fig. 16.Droop controller and supplementary controller output.

E. Case 5: Power Sharing with the Proposed Controller in Reduced System

The power sharing with the proposed controller in the reduced system is investigated in this section. DG-1 is disconnected first at 0.25 s when system is running in steady state. Fig. 17 shows the response and it can be seen that the other three DGs supply the extra power requirement. Ld_5 is disconnected at 1.3 s and the DG outputs reduce proportionally.

From the system response and numerical values (Appendix-A) it can be concluded that the DGs share the loads as desired while ensuring stable operation of the system.

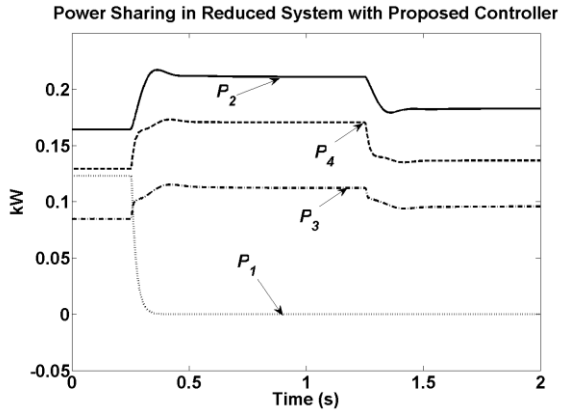


Fig. 17. System response for different system configuration.

To validate the performance of the supplementary proposed controller, the microgrid is operated similar situation as described in Case 2 with reduced system. Fig. 18 shows the system response. The proper power sharing (see Appendix A) with stable operation of the system indicates the efficacy of the proposed supplementary controller.

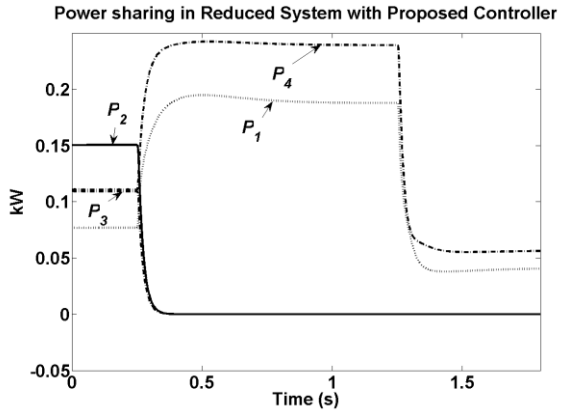


Fig. 18. Power sharing in reduced system.

VIII. Conclusions

Load sharing in an autonomous microgrid through angle droop control, instead of commonly used frequency droop, is investigated in this paper. High gain angle droop control ensures proper load sharing, especially under weak system conditions, but has a negative impact on the overall stability. This is illustrated through frequency domain modeling, eigenvalue analysis and time domain simulations. A supplementary loop is proposed around the primary droop control loop of each DG converter to stabilize the system despite having high gains that are required for better load sharing. The control loops are based on local power measurement and modulation of the d-axis voltage reference of each converter. The coordinated design of supplementary control loops for each DG is formulated as a parameter optimization problem and is solved using an evolutionary technique. The use of the supplementary droop control loop is shown to stabilize the system for a range of operating conditions while ensuring satisfactory load sharing.

Acknowledgement

The authors thank the Australian Research Council (ARC) for the financial support for this project through the ARC Discovery Grant DP 0774092 and also British Council for funding Dr Chauhuri's visits to QUT under the Researcher Exchange Program.

References

[1] M. C. Chandorkar, D. M. Divan and R. Adapa, "Control of parallel connected inverters in standalone ac supply systems," IEEE Trans. On Industry Applications, Vol. 29, No. 1, pp. 136-143, 1993.

[2] J. M. Guerrero, L. G. de Vicuna, J. Matas, M. Castilla, and J. Miret, "A wireless controller to enhance dynamic performance of parallel inverters in distributed generation systems," IEEE Trans. on Power Electronics, Vol. 19, No. 5, pp. 1205-1213, 2004.

[3] M. N. Marwali, M. Dai; A. Keyhani, "Robust stability analysis of voltage and current control for distributed generation systems" IEEE Trans. on Energy Conversion, Vol. 21, Issue-2, pp. 516-526, 2006.

[4] M. Reza, D. Sudarmadi, F. A. Viawan, W. L. Kling, and L. Van Der Sluis, "Dynamic Stability of Power Systems with Power Electronic Interfaced DG," Power Systems Conference and Exposition, PSCE'06, pp. 1423-1428, 2006.

[5] M. N. Marwali, M. Dai; A. Keyhani, "Stability Analysis of Load Sharing Control for Distributed Generation Systems," IEEE Trans. on Energy Conversion, Vol. 22, Issue-3, pp. 737-745, 2007.

[6] N. Pogaku, M. Prodanovic, T. C. Green, W. L. Kling, and L. Van Der Sluis, "Modeling, Analysis and Testing of Autonomous Operation of an Inverter-Based Microgrid," IEEE Trans. on Power Electronics, Vol. 22, Issue-2, pp. 613-625, 2007.

[7] J. G. Slootweg and W. L. Kling, "Impacts of distributed generation on power system transient stability," Power Engineering Society Summer Meeting, 2002 IEEE Vol. 2, No. , pp. 862-867, 2002.

[8] R. Majumder, A. Ghosh, G. Ledwich and F. Zare, "Load sharing and power quality enhanced operation of a distributed microgrid," IET Renewable Power Generation, Vol-2, No-3, pp 109-119, June, 2009, Current Issue, web http://www.ietdl.org/IET-RPG.

[9] R. E. Wilson, P. S. Sterlina, "GPS synchronized power system phase angle measurements", International Journal of Satellite Communications (ISSN 0737-2884), vol. 12, no. 5, p. 499-505.

[10] A. Ghosh and A. Joshi, "A new approach to load balancing and power factor correction in power distribution system," IEEE Trans. on Power Delivery, Vol. 15, No. 1, pp. 417-422, 2000.

[11] A.Ghosh and G. Ledwich, *Power Quality Enhancement using Custom Power Devices*, Kluwer's Power Electronics and Power System Series, Kluwer's Academic Publishers, Norwell, MA, 2002.

[12] N. Kroutikova, C. A. Hernandez-Aramburo, T. C. Green, "State-space model of grid-connected inverters under current control mode," IET Electric Power Applications, Vol. 1, No. 3, pp. 329-33, 2007.

[13] J.C.Geromel, J. Bernussou ,"Decentralized control through parameter space optimization." Automatica,1994 30(10): pp 1565-1578.

[14] A. L. B Do Bomfim,. G. N. Taranto (). "Simultaneous tuning of power system damping controllers using genetic algorithms." IEEE Transactions on Power Systems, 15(1), 2000: pp 163-169.

[15] J. Kennedy and R. Eberhart. "Particle swarm optimization.". Proceedings of IEEE International Conference on Neural Networks, 1995.

Appendix-A

Table-III: Numerical Results:

Case-1:Section VII.A **Full System of Fig. 6 with Lower Droop Gains: Fig.12 (a)**				
Power	Initial value	Final value	Times of P_{DG1} Initial	Times of P_{DG1} Final
P_{DG1}	0.077 MW	0.090 MW	1.0 (1.0)	1.0(1.0)
P_{DG2}	0.154 MW	0.168 MW	2.0(2.0)	**1.867**(2.0)
P_{DG3}	0.107 MW	0.119 MW	1.389(1.33)	1.32(1.33)
P_{DG4}	0.109 MW	0.124 MW	1.415(1.33)	1.378(1.33)

Case-2:Section VII.B Reduced System with Lower Droop Gains : Fig.13					
Power	Initial value	Interme-diate Value	Final value	Times of P_{DG1} Initial	Times of P_{DG1} Final
P_{DG1}	0.079 MW	0.198 MW	0.046 MW	1.0 (1.0)	1.0 (1.0)
P_{DG2}	0.154 MW	0 MW	0 MW	1.94 (2.0)	0.0 (0.0)
P_{DG3}	0.106 MW	0 MW	0 MW	1.34 (1.33)	0.0 (0.0)
P_{DG4}	0.108 MW	0.229 MW	0.051 MW	1.36 (1.33)	**1.108** (1.33)

Case-4: Section VII.D Power Sharing with the Proposed Supplementary Controller : Fig.15				
Power	Initial value	Final value	Times of P_{DG1} Initial	Times of P_{DG1} Final
P_{DG1}	0.078MW	0.064 MW	1.0 (1.0)	1.0 (1.0)
P_{DG2}	0.152 MW	0.129 MW	1.95 (2.0)	**2.02** (2.0)
P_{DG3}	0.107 MW	0.083 MW	1.36 (1.33)	1.29 (1.33)
P_{DG4}	0.108 MW	0.087 MW	1.37 (1.33)	1.35 (1.33)

Case-5:Section VII.E Power Sharing with the Proposed Controller in Reduced System:Fig.18					
Power	Initial value	Interme-diate value	Final value	Times of P_{DG1} Initial	Times of P_{DG1} Final
P_{DG1}	0.078 MW	0.188 MW	0.041 MW	1.0 (1.0)	1.0 (1.0)
P_{DG2}	0.152 MW	0.00 MW	0.0 MW	1.94 (2.0)	0.0 (0.0)
P_{DG3}	0.107 MW	0.0 MW	0.0 MW	1.36 (1.33)	0.0 (0.0)
P_{DG4}	0.108 MW	0.239 MW	0.055 MW	1.37 (1.33)	**1.342** (1.33)

Error in Power Sharing	Without Supplementary Controller	With Supplementary Controller
Overall Mean Error	**6.7 %**	**3.4%**
In reduced system	**14.8%**	**4.2%**

APPENDIX-B

Two show the relative differences between the angle and frequency droop controllers, we have chosen a simple system as shown in Fig. 4. The frequency droop controller is given by [1-4]

$$\omega = \omega_{ref} - m\left(P - P_{ref}\right) \tag{A.1}$$

The output impedances of the two sources are chosen in a ratio of 1:1.33 and the powers are also chosen in the ratio of 1.33:1. No reactive power droop has been used and the voltage magnitudes are held constant. Both frequency and angle droop controller gains are chosen at 50% of the marginal stability point. The VSCs and DGs ratings for both cases are assumed to be identical and the converter parameters are same as shown in Table-I.

The load in Fig. 1 is assumed to be resistive. To represent random changes of customer load, the conductance is chosen as the integral of a Gaussian white noise source. The output inductances of the converters are 30 mH and 22.6 mH. The impedance of line 1 is 0.25 + *j*1.3 while impedance of line 2 is 0.1 + *j*0.8. The steady state variation in the frequency for the two droop controllers are shown in Figs. 19 and 20. It can be seen that the frequency variation with the frequency droop controller is significantly higher than that with the angle droop controller. The standard deviation with the frequency droop controller is 0.151 rad/s, while the standard deviation with the angle droop controller is 0.0023 rad/s. It can also be seen that the mean frequency deviation is much larger in case of frequency droop than in angle droop. This demonstrates that the angle droop controller generates a substantially smaller frequency variation than the conventional frequency droop controller.

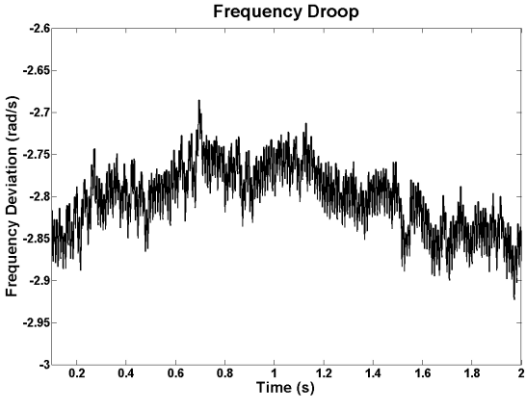


Fig. 19. Frequency variation with frequency droop control.

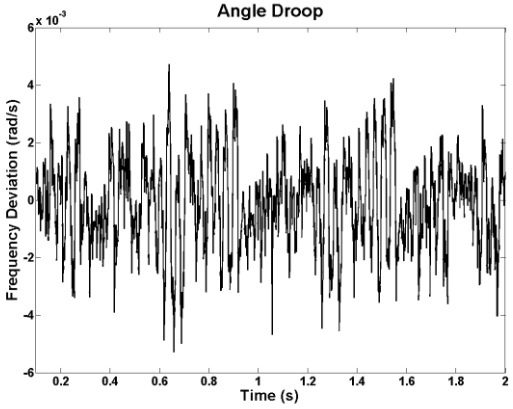


Fig. 20. Frequency variation with angle droop control.

The output power of DG-1 is shown in Fig. 21 for both frequency and angle droop controllers. Since the output powers in this figure are essentially the same and the DGs are operated at same constant voltage in both cases, the required current ratings of the VSCs are also same. As the load is not modeled as frequency dependant, the total power being supplied under both control schemes is also matched, as evident from Fig. 21. The improved performance of angle droop comes from a more responsive control. The switching frequency in both the cases is the same. Thus the converter requirements are the same in both the control schemes.

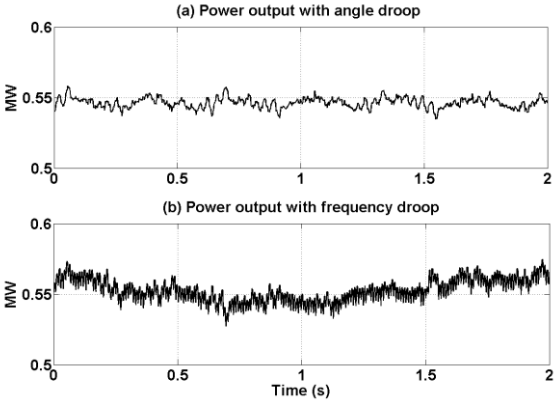


Fig. 21. Output power of DG-1for both droop control methods

Ritwik Majumder (S'07) received his B.E. in Electrical Engineering from Bengal Engineering College (Deemed University) in 2001 and his M.Sc. (Engg.) degree from Indian Institute of Science in 2004. From July 2004 to November 2004, he was with Tata Motor Engineering Research Centre in Jamshedpur, India. From November, 2004 to January 2006, he was with Siemens Automotive India and from January 2006 to May 2007, he was with ABB Corporate Research Centre, Bangalore, India. Since June 2007, he is a Ph.D. scholar in Queensland University of Technology. His interests are in Power Systems dynamics, Distributed Generation and Power Electronics Applications.

Balarko Chaudhuri (S'02–M'06) received the Ph.D. degree from Imperial College, London, U.K., in 2005.He was with GE Global Research from 2005 to 2006. Currently, he is a Lecturer with the Control and Power Group, Electrical and Electronic Engineering Department, Imperial College. His research interests are power system dynamics, stability, and control.

Arindam Ghosh (S'80, M'83, SM'93, F'06) is the Professor of Power Engineering at Queensland University of Technology, Brisbane, Australia. He has obtained a Ph.D. in EE from University of Calgary, Canada in 1983. Prior to joining the QUT in 2006, he was with the Dept. of Electrical Engineering at IIT Kanpur, India, for 21 years. He is a fellow of Indian National Academy of Engineering (INAE) and IEEE. His interests are in Control of Power Systems and Power Electronic devices.

Rajat Majumder (M'03) received the B.E. degree (first class honors) in electrical engineering from the Jadavpur University, Calcutta, India, the M.Sc.degree in electrical engineering from the Indian Institute of Science, Bangalore, India, in 2000 and 2003, respectively, and the Ph.D. degree from Imperial College, London, U.K., in 2006. Currently, he is a Scientist with the Corporate Research Center, ABB, Vasteras, Sweden. He was a Lecturer with the University of Queensland, Brisbane, Australia, from 2005 to 2007.

Gerard Ledwich (M'73, SM'92) received the Ph.D. in electrical engineering from the University of Newcastle, Australia, in 1976. He has been Chair Professor in Power Engineering at Queensland University of Technology, Australia since 2000. His interests are in the areas of power systems, power electronics, and controls. He is a Fellow of I.E.Aust.

Dr Firuz Zare (M'97, SM'06) was born in Iran in 1967. He holds a PhD degree in Electrical Engineering from Queensland University of Technology in Australia. He has worked as a development engineer and a consultant in industry for several years. He has joined the school of engineering systems in QUT in 2006. His research interests are power electronic applications, pulse-width modulation techniques, renewable energy systems and electromagnetic interferences.